Photoconductivity and Photolumniescence of $Al_{0.3}Ga_{0.7}As$/GaAs p-i-n Junction Quantum Well Solar Cells

David J. Christle

Physics and Mathematics, University of Minnesota-Twin Cities

NNIN iREU Site: National Institute for Materials Science (NIMS), Tsukuba, Ibaraki, Japan

NNIN iREU Principal Investigator(s): Prof. Hiroyuki Sakaki, NIMS, Quantum Dot Research Center; Toyota Technological Institute, 201201 Hisakata, Tempaku-ku, Nagoya 468-8511, Japan

NNIN iREU Mentor(s): Dr. Takeshi Noda, National Institute for Materials Science, Quantum Dot Research Center, 1-2-1 Sengen, Tsukuba, Ibaraki 305-0047, Japan

Contact: christle@cnsi.ucsb.edu, h-sakaki@toyota-ti.ac.jp, noda.takeshi@nims.go.jp

Abstract:

Single-junction gallium arsenide (GaAs) photovoltaic devices are thermodynamically limited to roughly 30% efficiencies in Air Mass (AM) 1.5 conditions via the well-known Shockley-Quesslier limit. Under idealistic assumptions, a photovoltaic device containing an intermediate energy band between the edges of the conduction and valence bands has been shown to have an efficiency limit upwards of 60%, primarily due to the absorption of sub-bandgap photons [1]. An $Al_{0.3}Ga_{0.7}As$/GaAs-based quantum well solar cell realizes this special electronic structure by alternating growth layers between $Al_{0.3}Ga_{0.7}As$ (E_g = 1.8 eV) and GaAs (E_g = 1.42 eV). This growth of repeating heterojunctions forms a series of quantum wells (QWs) known as a superlattice, which admits a large number of bound states at energies between the GaAs/$Al_{0.3}Ga_{0.7}As$ band edges. Adjusting the width and separation of these quantum wells controls both the width and the depth of this intermediate band, meaning this technique is also tunable.

Introduction and Experimental Procedure:

In this paper, we attempt to understand the dynamics of photogenerated carriers in such a device by measuring the photoconductivity and photoluminescence of $Al_{0.3}Ga_{0.7}As$/GaAs quantum wells embedded in the intrinsic region of standard p-i-n junction solar cells. These measurements are germane since carriers can either be swept away by the internal electric field, creating a current, or recombine radiatively or non-radiatively, with the former being observed as photoluminescence.

We grew four films with 1, 10, 25 and 50 quantum wells, along with a control sample containing no quantum wells, via molecular beam epitaxy. All films were grown on an *n*-type GaAs (100) substrate at a substrate temperature (temp) of 580-600°C, and consisted of 300 nm *n*-GaAs ($n = 1 \times 10^{18}$ cm^{-3}), and 300 nm of *n*-$Al_{0.3}Ga_{0.7}As$ ($n = 5 \times 10^{17}$ cm^{-3}) for the n-doped region. The intrinsic region was a variable layer of 150 nm to 493 nm of *i*-$Al_{0.3}Ga_{0.7}As$ with repeated pair layers of 3 nm *i*-$Al_{0.3}Ga_{0.7}As$ and 4 nm *i*-GaAs to create *N* QWs, and 500 nm of *i*-$Al_{0.3}Ga_{0.7}As$.

The variable layer thickness was adjusted so that the entire intrinsic region thickness was fixed at 1 μm in all samples. The top *p*-region was 200 nm *p*-$Al_{0.3}Ga_{0.7}As$ ($p = 5 \times 10^{17}$ cm^{-3}), 20 nm *p*-$Al_{0.3}Ga_{0.7}As$ ($p = 2 \times 10^{18}$ cm^{-3}), and 20 nm of *p*-GaAs ($p = 2 \times 10^{19}$ cm^{-3}). A 20 nm, 1 mm diameter chromium gold (CrAu) ring was patterned by photolithography and deposited using thermal deposition. We used a wet etch to create a mesa structure and finally made electrical contact by pressing indium or Au wedge bonding.

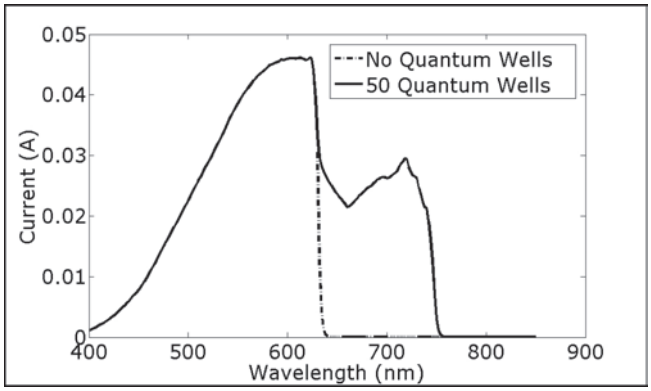

Figure 1: A plot of data obtained from the 50 QW sample versus the control.

In our photocurrent apparatus, a halogen lamp light was incident through a slit into a standard monochromator that emitted monochromatic light with a spectral width of ≈ 3 nm. The light was modulated via a mechanical chopper and lens-focused onto the mesa of the sample, which was mounted in a nitrogen flow cryostat. We used an SR530 lock-in amplifier in current-sensing mode to recover the emitted current due to photovoltaic action. We scanned the monochromator wavelength from 400 nm to 850 nm and measured the current through the device to produce spectra as in Figure 1.

Our photoluminescence apparatus consisted of a fiber-coupled Andor iDus spectrometer lens—focused to samples mounted in a closed-cycle (6-300 K) cryostat. A 550 nm laser at oblique incidence excited carriers within the $Al_{0.3}Ga_{0.7}As$

region, which diffused and relaxed into the QWs where they may radiatively recombine.

Figure 4 shows the AM 1.5 I-V characteristics of our devices that had an expected increase in the short-circuit current I_{sc} roughly linear with the number of QWs in accordance with sub-bandgap absorption, with the 50 QW sample showing a ~ 45% increase. We also observed a reduction in the open-circuit voltage that kept each device's efficiency near 10%.

Results and Conclusions:

We discuss in detail here photoluminescence for the 25 QW sample since it had the most complete dataset. PL spectra versus temp showed the QW emission peak energy decreased with increasing temp for all QW samples, and that this decrease was Varshni-like for the 25 QW sample.

An Arrhenius plot of PL versus temp in Figure 3 shows significant thermal quenching of the integrated PL intensity for the same sample. The behavior is well-described by a Boltzmann three-level model with activation energies of (27.7 ± 1.2) meV and (119 ± 6) meV. The low-energy quenching mechanism is unclear to us, however other groups with similar structures attribute a similar activation energy to thermal delocalization of excitons trapped in potential fluctuations of the well layers [2,3]. The high energy quenching mechanism we attribute to carrier thermal escape, since this energy is consistent with our theoretical band structure calculations [2,4]. Our data show the low-energy quenching mechanism is more pronounced than quenching associated with thermal escape. Quenching is observed qualitatively in all samples.

Measuring the photocurrent served as a probe of the underlying energy-dependent device physics. We first extracted the higher energy full-width half-maximum wavelength from the photoluminescence data. We then calculated the ratio between the spectrum-corrected photocurrent at this energy and the top of the band edge associated with $Al_{0.3}Ga_{0.7}As$, which had negligible temp dependence, to eliminate measurement-to-measurement light intensity fluctuations. Measurement at the upper FWHM energy corrected for the Stokes shift, the energy difference between the emission peak and the effective QW joint density of states edge observed in semiconductors with alloy disorder [5].

Figure 2 shows a semilogarithmic plot of this ratio versus temp. The single and ten QW samples both show saturation with increasing temp, while both the 25 and 50 QW samples are saturated above 77 K. The PL intensity for the 25 QW sample shows an order of magnitude decrease in radiative recombination while the photocurrent remains essentially constant, indicating that excitons previously localized by potential fluctuations in the well structures instead undergo a non-radiative recombination process unidentified in the present experiment. We also observe what appears to be an increase in the photocurrent with decreasing temp near 77-90 K in the unsaturated samples, the unclear origin of which requires more investigation.

We have characterized the photoluminescence and photocurrent properties of QW and multi-QW $Al_{0.3}Ga_{0.7}As/GaAs$ solar cells in addition to observing a promising increase in the short-circuit current. We have measured two distinct thermally-activated quenching mechanisms and highlighted future avenues of investigation into understanding the physics of these and other confinement-based devices, such as the quantum dot solar cell.

Acknowledgements:

David Christle would like to gratefully acknowledge mentor Dr. T. Noda, Dr. T. Mano, and principal investigator Dr. H. Sakaki for their generous support and tutelage throughout the program. This work was supported by the NSF, NIMS, and the NNIN iREU program.

References:

[1] A. Luque and A. Marti, Phys. Rev. Lett. 78 (1997).
[2] I. Friel et al., Appl. Phys. Lett. 85, 3068 (2004).
[3] J. D. Lambkin et al., Appl. Phys. Lett. 56 (1990).
[4] S. Birner et al., IEEE T. Electron. Dev. 54 (2007).
[5] M. Gurioli et al., Phys. Rev. B 50 (1994).

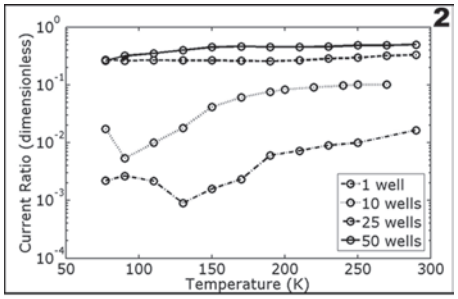

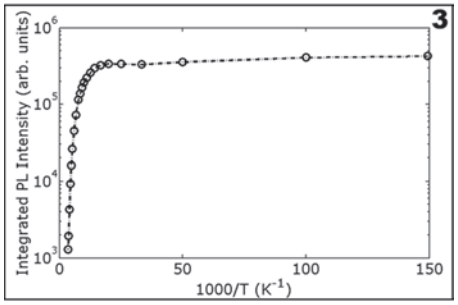

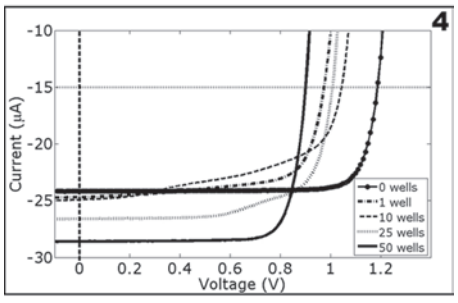

Figure 2: A semilogarthmic plot of the ratio between the upper FWHM and band-edge currents.

Figure 3: An Arrhenius plot for the 25 QW sample photoluminescence intensity.

Figure 4: I-V characteristics in AM 1.5 conditions. Dashed and dotted axes aide in showing the short-circuit current/open-circuit voltages.